Optimization Under Uncertainty of the Acquisition Plan of Earth Observation Satellites

EL AMRANI Wadie[1], RATABOUIL Guilhem[1], FARGIER Hélène[1,2]

[1]University of Toulouse III, Paul Sabatier, Toulouse, France
[2]IRIT, Toulouse, France

Résumé We address the problem of optimizing the acquisition plan of Earth Observation Satellites (EOSs) under uncertainty due to cloud coverage and instrument failures. We formulate the scheduling problem as a Binary Integer Programming (BIP) model, incorporating uncertainties using imprecise probability frameworks from decision theory. Specifically, we define pessimistic and optimistic expected utilities to model the decision-maker's preferences under uncertainty. We implement the model using Zimpl and solve it with SCIP, testing it on five datasets with varying characteristics. Our results demonstrate that considering uncertainties significantly impacts the optimal scheduling decisions, highlighting the importance of robust optimization in EOS mission planning. Our implementation is available at https://github.com/paul-sabatier-research-projects/Satellite-planning-under-uncertainty.

Keywords: Earth Observation Satellites · Uncertainty · Optimization · Decision Theory · Binary Integer Programming

1 Introduction

Earth observation satellites (EOSs) are platforms equipped with sensors that orbit the Earth to take photographs of specific areas at the request of users [1,2]. EOSs can capture images while moving along their orbits. The SPOT series constitutes a family of these observation satellites, which are developed by CNES (French Centre National d'Etudes Spatiales) and operated by the SPOT Image company [3] (see Fig 1).

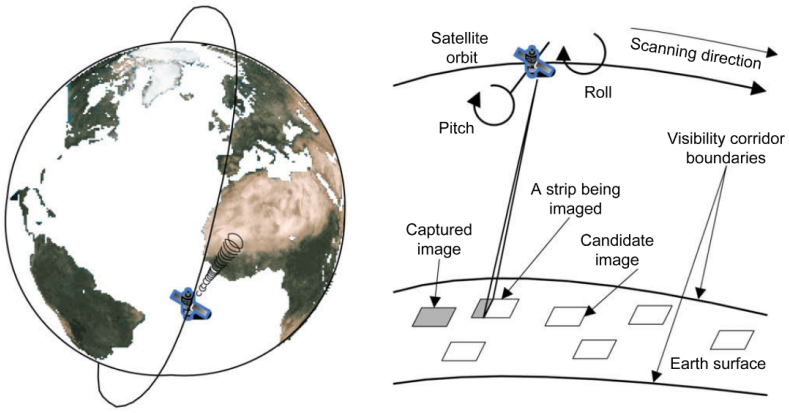

(a) SPOT5 orbit. (b) A photograph acquisition.

FIGURE 1 – Photograph acquisition performed by SPOT5 [4].

After capturing the photographs, the acquired data are stored in the onboard limited memory and transferred to a ground station when the satellites are within feasible transferring range (see Fig 3). Most EOSs operate at low altitudes with orbital periods of dozens of minutes or several hours. The SPOT-5 satellite's has three optical instruments, High Resolution Stereoscopic (HRS), Vegetation, and High Resolution Geometric (HRG), are pointed in forward, nadir, and backward directions, respectively (ie Fig 2). This configuration allows SPOT-5 to achieve comprehensive and high-resolution Earth observation capabilities, supporting various applications from topographical mapping to vegetation monitoring. Mono-images require any one of the three instruments. Stereo images need both the (HRS) and (HRG) [5]. If possible, the image data are directly transmitted to a

ground reception station. Otherwise, they are stored using onboard recorders and downlinked when the satellite is within range of a reception station. The SPOT Image company receives imaging requests from clients worldwide and strives to satisfy them as best as possible. Both long-term and short-term system management strategies are used for this purpose. The problem we present is the short-term management problem, which consists of deciding each day which images will be taken the next day and how to take them.

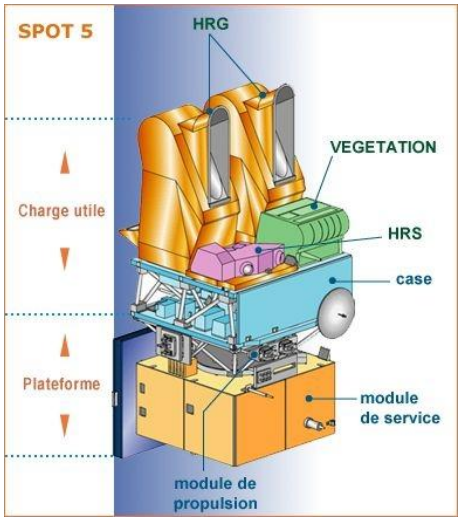

FIGURE 2 – Schematic view of the SPOT5 architecture (image credit : CNES)

The mission planning problem of an EOS is concerned with maximizing a profit function subject to a set of satellite capacity constraints over the planning horizon. It can be defined as the selection of a subset of photographs from a candidate set in order to satisfy a maximal profit of the requested photographs (ie. Fig 1b). The problem contains a number of decision variables and constraints making it a combinatorial optimization problem that is typically solved using heuristics [4].

The acquisition can be performed using multiple satellites ; however, this paper focuses on decision-making for a single satellite. We believe that solving the problem for one satellite can later be extended to multiple satellites. Given prior knowledge of client demands, such as requested images, our goal is to select the best images to acquire. The feasibility of acquiring these images depends on various constraints, including the configuration of the three instruments and the required angle rotations for each instrument, which are determined by the mirrors' angular velocity. The start date of acquisition depends solely on when the satellite traverses the target zone and the necessary angle. If the start times of two images overlap, the same instrument cannot capture both images on the same day. Furthermore, the problem involves not only deciding which images to acquire but also determining which instrument to use.

Extensive research has been carried out on the deterministic EOS scheduling problem [7,8,9]. However, limited attention has been paid to uncertainty, which can significantly influence Earth observation missions. Wang et al. [10] introduced a chance-constrained programming model to represent cloud coverage uncertainty and adopted a sample approximation method to solve the problem. Xinwei et al. [11] introduced the concept of a budgeted uncertainty set and established a linearized robust scheduling model, where the budget value is determined by satellite operation costs and the degree of conservatism. Uncertainty is inevitable and may also arise from satellite system failures of instruments [12]. In this paper, we address uncertainty by considering the probability of cloudy images and instrument failures. In the next section, we discuss the rigorous formulation of the problem.

To rigorously model this uncertainty, we employ frameworks from decision theory under uncertainty, as developed by pioneers like Leonard J. Savage [13], Abraham Wald [14], and Daniel Ellsberg [15]. These theories consider situations where probabilities are imprecise or unknown, leading to the development of concepts such as maximin and minimax criteria, and the introduction of imprecise probabilities. We also draw upon the work of Lotfi A. Zadeh [16] on possibility theory and George A. Papadopoulos [17] on decision-making under uncertainty. In the first section,

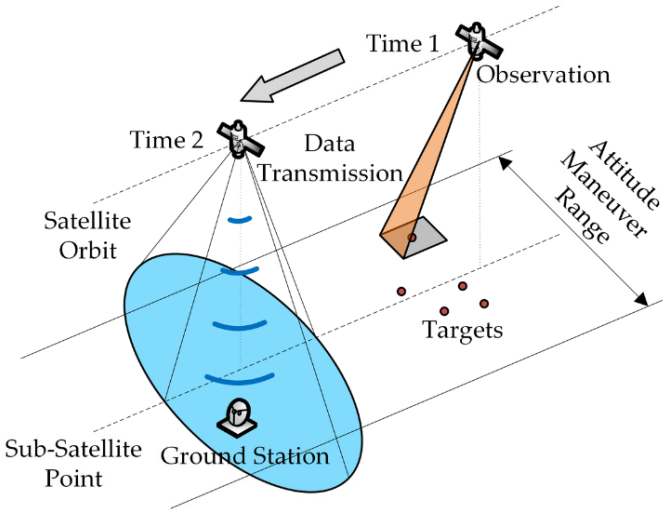

FIGURE 3 – Schematic representation of satellite operations during two observation and data transmission phases. At Time 1, the satellite captures images of targets within its attitude maneuver range as it orbits over a ground station. By Time 2, it transmits the gathered data back to the same ground station, indicating the process of data flow from observation to ground reception [6].

we model our decision problem without taking into account the uncertainties. Then, in the third section, we consider the uncertainties and see how we can model the decision-maker using the imprecise probability framework. By integrating these theoretical foundations, we aim to create a more robust decision-making model that can effectively handle the uncertainties inherent in cloud coverage and instrument reliability

2 Problem Description

2.1 Datasets and Parameters

We have five datasets, named *SPOT1* to *SPOT5*, each with varying characteristics. The datasets differ in the number of images, types of images (mono or stereo), the duration needed to acquire any image ($\boldsymbol{DU}$), the angular velocity of the mirror rotation ($\boldsymbol{VI}$), the memory capacity ($\boldsymbol{PM}_{\max}$), and the presence of uncertainties in instrument failure and cloud coverage. Table 1 summarizes the key characteristics of each dataset.

Dataset	**Images**		**Memory Capacity** ($\boldsymbol{PM}_{\max}$)	**Duration** ($\boldsymbol{DU}$ s)	**Angular Velocity** ($\boldsymbol{VI}$ deg/s)	**Instrument Failure**	**Cloud Uncertainty**
	Mono	**Stereo**					
SPOT1	2	1	35	20	1	✗	✓
SPOT2	2	1	35	20	1	✗	✗
SPOT3	2	1	50	100	1	✗	✗
SPOT4	14	6	150	20	1	✗	✓
SPOT5	26	14	300	20	1	✓	✓

TABLE 1 – Summary of Datasets Used in Experiments

We provide detailed tables for the memory size required for each image ($\boldsymbol{pm_i}$), the acquisition dates ($\boldsymbol{dd_{i,j}}$), the depointing angles ($\boldsymbol{an_{i,j}}$), and the angular velocity ($\boldsymbol{VI}$), but only for *SPOT1*, as the other datasets are similar.

We focus on the short-term scheduling of image acquisitions by a single satellite within one day. Let $\boldsymbol{s}_{\text{im}} = \{1, 2, \ldots, n\}$ denote the set of image indices, where n is the total number of requested

images. Each image $i \in \boldsymbol{s}_{\text{im}}$ is classified as either mono or stereo, indicated by $\boldsymbol{ty_i} = 1$ for mono or $\boldsymbol{ty_i} = 2$ for stereo. The satellite is equipped with a set of instruments $\boldsymbol{s}_{\text{ins}} = \{1, 2, 3\}$.

Each image i requires a specific memory size $\boldsymbol{pm_i}$ and has an associated price $\boldsymbol{pa_i}$ for acquisition. The acquisition time for image i using instrument j is denoted by $\boldsymbol{dd_{i,j}}$. These acquisition times are organized in the bidimensional table $\boldsymbol{dd_{i,j}}$, where i ranges over images and $j \in \boldsymbol{s}_{\text{ins}}$. Additionally, each image acquisition requires a fixed depointing angle $\boldsymbol{an_{i,j}}$ (in degrees) for instrument j, stored in the bidimensional table $\boldsymbol{an_{i,j}}$.

The duration needed to acquire any image is a constant $\boldsymbol{DU}$ (in seconds), and the angular velocity of the mirror rotation is $\boldsymbol{VI}$ (degrees per second). The start time $\boldsymbol{t_0} = 0$ seconds marks the beginning of the satellite's orbital revolution.

We consider uncertainties related to cloud coverage and instrument failure. Each image i has associated lower and upper probabilities $\boldsymbol{p}_{\text{inf},\boldsymbol{i}}$ and $\boldsymbol{p}_{\text{sup},\boldsymbol{i}}$ of being cloudy. Each instrument j has a probability $\boldsymbol{p_j}$ of failure.

The notations used in the problem formulation are summarized in Table 2.

Symbol	Description
$\boldsymbol{i}$	Index representing images, $i \in \{1, \ldots, n\}$
$\boldsymbol{j}$	Index representing instruments, $j \in \{1, 2, 3\}$
$\boldsymbol{s}_{\text{im}}$	Set of image indices i
$\boldsymbol{s}_{\text{ins}}$	Set of instruments on the satellite
$\boldsymbol{DU}$	Duration needed for image acquisition (seconds)
$\boldsymbol{VI}$	Angular velocity of mirror rotation (degrees/second)
$\boldsymbol{ty_i}$	Type of image i : 1 for mono, 2 for stereo
$\boldsymbol{pm_i}$	Memory size required for image i
$\boldsymbol{pa_i}$	Price associated with acquiring image i
$\boldsymbol{p}_{\text{inf},\boldsymbol{i}}$	Lower probability of image i being cloudy
$\boldsymbol{p}_{\text{sup},\boldsymbol{i}}$	Upper probability of image i being cloudy
$\boldsymbol{p_j}$	Failure probability of instrument j
$\boldsymbol{dd_{i,j}}$	Acquisition date of image i with instrument j
$\boldsymbol{an_{i,j}}$	Depointing angle for acquiring image i with instrument j (degrees)
$\boldsymbol{t_0}$	Start time of satellite's orbital revolution (seconds)

Table 2 – Notations Used in the Problem Formulation

Example The tables below show an example of the available parameters for *SPOT1*.

Table 3 – Image Parameters for SPOT1

Image	$\boldsymbol{ty_i}$	$\boldsymbol{pm_i}$	$\boldsymbol{pa_i}$	$\boldsymbol{p}_{\text{inf},\boldsymbol{i}}$	$\boldsymbol{p}_{\text{sup},\boldsymbol{i}}$
1	1 (Mono)	10	10	0	0.1
2	2 (Stereo)	20	20	0	0.2
3	1 (Mono)	10	40	0	0.3

Table 4 – Acquisition Dates $\boldsymbol{dd_{i,j}}$ for SPOT1 (in seconds)

Image	$\boldsymbol{dd_{i,1}}$	$\boldsymbol{dd_{i,2}}$	$\boldsymbol{dd_{i,3}}$
1	130	230	330
2	150	0	350
3	220	320	420

2.2 An Optimization Scheduling Problem

Without loss of generalization, lets take SPOT1 as an example, we deal with scheduling image acquisitions for three images using three instruments on a satellite. The starting dates for each image on each instrument are predetermined based on the satellite's trajectory and the geographical locations of the target images (see Fig 2). The acquisition duration for each image is a fixed constant $\boldsymbol{DU} = 20$ seconds.

TABLE 5 – Depointing Angles $an_{i,j}$ for SPOT1 (in degrees)

Image	$an_{i,1}$	$an_{i,2}$	$an_{i,3}$
1	0	10	10
2	5	0	5
3	20	20	20

TABLE 6 – Instrument Failure Probabilities for SPOT1

Instrument	p_j
1	0
2	0
3	0

Table 7 provides the starting dates for each image on each instrument. An entry of zero indicates that the image cannot be acquired using that instrument.

Image	Instrument 1	Instrument 2	Instrument 3
1	130	230	330
2	150	0	350
3	220	320	420

TABLE 7 – Starting Dates $dd_{i,j}$ for SPOT1 (in seconds)

To visualize the scheduling problem, we create a Gantt chart (Figure 7) that represents the acquisition periods for each image on the available instruments. Each rectangle corresponds to the time interval during which an image is being acquired by an instrument. The rectangles start at the specified starting dates and have a duration equal to DU.

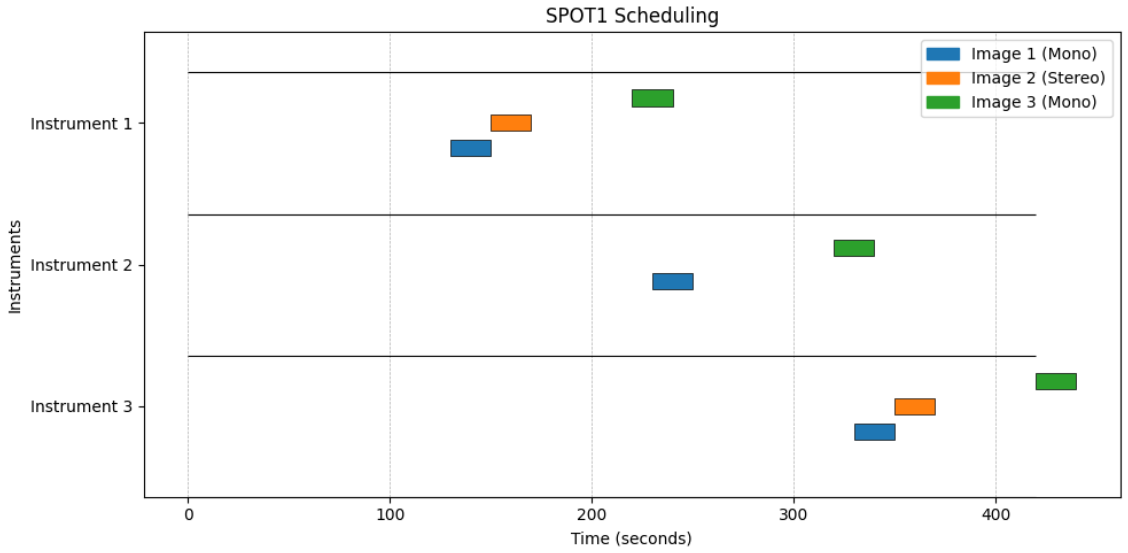

FIGURE 4 – Gantt Chart for SPOT1 Image Acquisitions

We approach the problem using a hierarchical model of constraints, as illustrated in Figure 5. The outermost circle represents the initial solution space where all images can be scheduled without overlapping acquisition times. Adding the mirror adjustment constraint reduces the solution space, as the time needed to adjust the instrument's mirror between images may prevent certain sequences. The memory capacity constraint further narrows the feasible solutions. Our aim is not to create an optimization solution but to intuitively build an approach to solve the problem using the Gantt chart and constraints. While the scheduling decisions are evident in the case of three images, the complexity of the problem increases exponentially as the number of images and instruments grows. It's clear that transitioning from the memory capacity constraint to maximizing the total profit

corresponds to solving a knapsack problem, which is known to be NP-complete. Therefore, finding the optimal schedule for larger instances becomes computationally challenging without advanced optimization techniques. This will be discussed in the next sections ; for now, let's build an intuitive understanding of the problem.

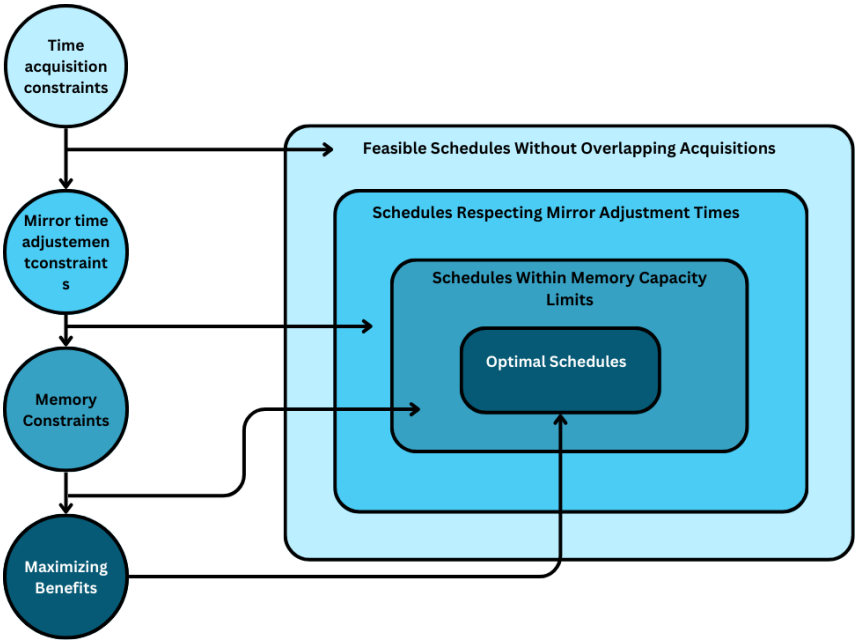

FIGURE 5 – Hierarchical Model of Constraints

Each image acquisition requires time for capturing the image and adjusting the mirror to the required depointing angle (Figure 6). The time to adjust the mirror from angle θ_{img1} to θ_{img2} is :

$$T_{\text{adjust}} = \frac{|\theta_{\text{img2}} - \theta_{\text{img1}}|}{\text{VI}},$$

where VI is the angular velocity of the mirror (degrees per second).

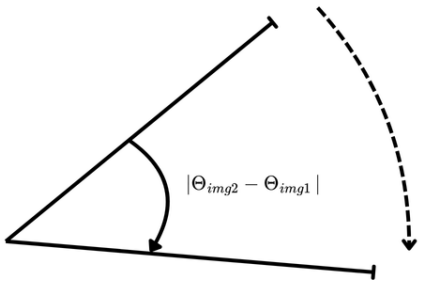

FIGURE 6 – Mirror adjustment from angle θ_{img1} to θ_{img2} requires time T_{adjust}

The total time between starting the acquisition of the first image and being ready to start the second is :

$$T_{\text{total}} = \text{DU} + T_{\text{adjust}}.$$

To avoid scheduling conflicts between two images assigned to the same instrument, the following constraint must be satisfied :

$$|\text{startDate}_{\text{img2}} - \text{startDate}_{\text{img1}}| \geq T_{\text{total}}.$$

If this condition is not met, it is not feasible to acquire both images in succession with the same instrument. For example, instrument 1 cannot acquire image 2 if we choose to acquire image 1

(Figure 7) because we do not have enough time to adjust the mirror from angle 0° to 5° (Table 5). However, it is possible for instrument 1 to acquire image 3 after image 2, since :

$$T_{\text{adjust}} = \frac{|\theta_3 - \theta_2|}{\text{VI}} = \frac{|20° - 5°|}{1°/\text{s}} = 15\,\text{s},$$

$$\text{startDate}_3 - \text{startDate}_2 = 220\,\text{s} - 150\,\text{s} = 70\,\text{s},$$

and

$$T_{\text{total}} = \text{DU} + T_{\text{adjust}} = 20\,\text{s} + 15\,\text{s} = 35\,\text{s} < 70\,\text{s}.$$

Thus, the mirror adjustment constraint is satisfied.

Considering the memory capacity constraint ($\boldsymbol{PM}_{\max} = 35$), the solution space becomes smaller. The total memory required for the images must not exceed this limit. The possible combinations of images that satisfy the memory constraint are :

- Image 1 and Image 2 : $10 + 20 = 30 \leq 35$ - Image 1 and Image 3 : $10 + 10 = 20 \leq 35$ - Image 2 and Image 3 : $20 + 10 = 30 \leq 35$

Our goal is to choose the combination that maximizes the total profit. Since Image 3 has the highest profit value ($\boldsymbol{pa_3} = 40$), selecting Image 3 along with either Image 1 or Image 2 is optimal under the memory constraint.

Combination	Images	Instrument Assignments	Total Memory	Profit	Feasible
1	Image 1	Instr. 1 or 2 or 3	10	10	Yes
2	Image 2	Instr. 1 or 3	20	20	Yes
3	Image 3	Instr. 1 or 2 or 3	10	40	Yes
4	Images 1 & 2	Image 1 : Instr. 1, Image 2 : Instr. 3	30	30	Yes
5	Images 1 & 3	Both on Instr. 1	20	50	Yes
6	Images 2 & 3	Image 2 : Instr. (1,3), Image 3 : Instr. 1	30	60	Yes
7	Images 1, 2 & 3	–	40	70	No

TABLE 8 – Possible Scheduling Solutions for SPOT1

For *SPOT3*, although the memory capacity ($\boldsymbol{PM}_{\max} = 50$) allows acquiring all images, the acquisition duration is increased to $\boldsymbol{DU} = 100$ seconds. This results in overlapping acquisition times on each instrument, making it possible to take only one image per instrument(Figure 7). Therefore, we need to select images that maximize the profit while respecting the time constraints.

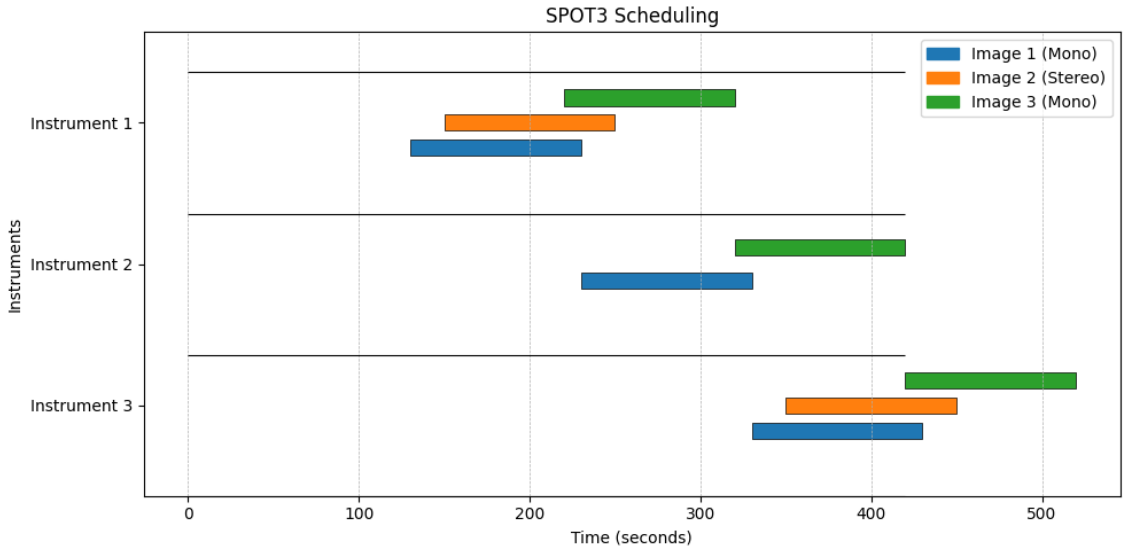

FIGURE 7 – Gantt Chart for SPOT3 Image Acquisitions

3 Problem Under Uncertainty

The problem of uncertainty arises from two main sources. The first is intrinsic to the satellite, represented by a constant probability of failure p_j for instrument j. The second source stems from image cloudiness, where we define a range of possible probabilities for each image, modeled as a set $\mathcal{F}_i = \{p_i \mid p_i \in [p_{\text{inf}}, p_{\text{sup}}]\}$. Therefore, the exact probability of cloudiness is unknown ; instead, the decision-maker's knowledge is represented by a set of probability measures.

FIGURE 8 – Decision-Making Under Uncertainty

Consider a scenario where two solutions are feasible : selecting images (1,2) or (2,3), both yielding the same profit.

Image	ty_i	pm_i	pa_i	$p_{\text{inf},i}$	$p_{\text{sup},i}$
1	1 (Mono)	10	10	0	0.1
2	2 (Stereo)	20	20	0	0.2
3	1 (Mono)	10	10	0	0.3

TABLE 9 – Image Parameters Example

A rational decision-maker would prefer the solution (1,2) over (2,3) because image 1 has a lower upper bound on cloudiness probability than image 3, i.e., $p_{\text{sup},1} < p_{\text{sup},3}$. With equal profit, there is no incentive to risk.

However, the decision-maker may consider taking a risk if image 3 offers a higher profit than image 1, as illustrated in the SPOT1 example below :

Image	ty_i	pm_i	pa_i	$p_{\text{inf},i}$	$p_{\text{sup},i}$
1	1 (Mono)	10	10	0	0.1
2	2 (Stereo)	20	20	0	0.2
3	1 (Mono)	10	40	0	0.3

TABLE 10 – Image Parameters Example for SPOT1

Since the actual probability of cloudiness is not known precisely, but only within a defined range, we are dealing with imprecise probabilities. In this section, we will introduce key concepts from decision theory to rigorously model this uncertainty.

3.1 Utility Function

We suppose that the decision maker has ordered preferences across the consequences of their decisions. In our case, if an image is sold—that is, successfully acquired and not cloudy—the gain is its price. If not (in the case of a cloudy image or instrument failure), the image cannot be sold, so its gain is set to 0. Formally, we define the function $u : X \to \mathbb{R}$ for each image, such that $X = \{\text{sold image}, \text{unsold image}\}$, and :

$$u(\text{sold image}) = \text{Price of image}, \quad u(\text{unsold image}) = 0.$$

Our utility is simply the gain.

3.2 Expected Utility

In our case, the beliefs of the decision maker can be represented with a probability measure derived from observations of a random phenomenon (failure of instruments or cloudy images). The choice of decisions can then be based on the expected utility defined as :

$$\text{Maximize} \quad \text{EU}_p(d) = \sum_s p(s) \cdot u(d(s)),$$

where $d(s)$ is the gain from event s (possibly sold image or corrupted image).

In our case, since $u(x) = x$, the expected utility simplifies to :

$$\text{EU}_p(d) = \sum_s p(s) \cdot d(s).$$

Here, we must emphasize the difference between the instrument uncertainty and the cloudiness uncertainty. In the case of instruments, $p(s)$ is a constant value, but for cloudiness, p is a set of values. In the literature, this is often referred to as the *credal set*.

3.3 Lower and Upper Bounds

This concept will be used in the context of cloudy images. Given a credal set $\mathcal{F}$, the lower and upper probabilities are defined as :

$$P_*(A) = \inf_{p \in \mathcal{F}} P(A), \quad P^*(A) = \sup_{p \in \mathcal{F}} P(A).$$

In our case, for the event of an image being cloudy, we have :

$$P_*(\text{cloudy}) = p_{\text{inf}}, \quad P^*(\text{cloudy}) = p_{\text{sup}}.$$

To make decisions under uncertainty with imprecise probabilities.

we can use the ***Pessimistic expected utility***, which considers the worst-case scenario within the credal set :

$$\text{UE}_*(f) = \inf_{p \in \mathcal{F}} \text{EU}_p(f).$$

Similarly, the ***Optimistic expected utility*** considers the best-case scenario :

$$\text{UE} *_(f) = \sup_{p \in \mathcal{F}} \text{EU}_p(f).$$

3.4 The Model

We model the uncertainty of cloudy images and instrument failure within the same probability framework. We define the set of possible states $\mathcal{F}_{i,j}$ as :

$$\mathcal{F}_{i,j} = \{(\omega_i, \omega_j) \mid \omega_i \in \{\text{Cloudy}_i, \overline{\text{Cloudy}}_i\},\ \omega_j \in \{\text{OK}_j, \overline{\text{OK}}_j\}\}.$$

Here, $\overline{\text{Cloudy}}_i$ denotes the complement of the event Cloudy_i, i.e., the image i is not cloudy. Similarly, $\overline{\text{OK}}_j$ denotes the event where instrument j is not functioning properly.

Our expected utility under the pessimistic criterion is defined as :

$$\text{UE}_*(d) = \inf_{p_{i,j} \in \mathcal{F}_{i,j}} \sum_{s \in S} p_{i,j}(s) \cdot u(d(s)).$$

Since $u(x) = x$, this simplifies to :

$$\text{UE}_*(d) = \inf_{p_{i,j} \in \mathcal{F}_{i,j}} \sum_{s \in S} p_{i,j}(s) \cdot d(s).$$

In our model, the utility $d(s)$ is pa_i (the price of image i) if the state $s = (\overline{\text{Cloudy}}_i, \text{OK}_j)$, and 0 otherwise. Therefore :

$$\text{UE}_*(d) = \inf_{p_{i,j} \in \mathcal{F}_{i,j}} \left[p\left(\overline{\text{Cloudy}}_i, \text{OK}_j\right) \cdot pa_i + \sum_{\substack{s \in S \\ s \neq (\overline{\text{Cloudy}}_i, \text{OK}_j)}} p(s) \cdot 0 \right].$$

Simplifying, we get :

$$\text{UE}_*(d) = \inf_{p_{i,j} \in \mathcal{F}_{i,j}} p\left(\overline{\text{Cloudy}}_i, \text{OK}_j\right) \cdot pa_i.$$

Since the events are independent :

$$p\left(\overline{\text{Cloudy}}_i, \text{OK}_j\right) = (1 - p_i) \cdot (1 - p_j).$$

Substituting back into the expected utility, we have :

$$\text{UE}_*(d) = \inf_{\substack{p_i \in [p_{\text{inf}}, p_{\text{sup}}] \\ p_j}} \left[(1 - p_i) \cdot (1 - p_j) \cdot pa_i\right].$$

We can factor out $(1 - p_j) \cdot pa_i$ since they are constants :

$$\text{UE}_*(d) = (1 - p_j) \cdot pa_i \cdot \inf_{p_i \in [p_{\text{inf}}, p_{\text{sup}}]} (1 - p_i).$$

Since $(1 - p_i)$ is decreasing in p_i, the infimum occurs at $p_i = p_{\text{sup}}$:

$$\inf_{p_i \in [p_{\text{inf}}, p_{\text{sup}}]} (1 - p_i) = 1 - p_{\text{sup}}.$$

Thus, the pessimistic expected utility becomes :

$$\text{UE}_*(d) = (1 - p_j) \cdot pa_i \cdot (1 - p_{\text{sup}}).$$

Similarly, the optimistic expected utility is :

$$\text{UE}^*(d) = (1 - p_j) \cdot pa_i \cdot \sup_{p_i \in [p_{\text{inf}}, p_{\text{sup}}]} (1 - p_i).$$

Since $(1 - p_i)$ is decreasing in p_i, the supremum occurs at $p_i = p_{\text{inf}}$:

$$\sup_{p_i \in [p_{\text{inf}}, p_{\text{sup}}]} (1 - p_i) = 1 - p_{\text{inf}}.$$

Therefore :

$$\text{UE}^*(d) = (1 - p_j) \cdot pa_i \cdot (1 - p_{\text{inf}}).$$

This development shows that the expected utility depends on p_i, and since p_j is a constant, we can separate p_i and p_j under the infimum (or supremum). Specifically, we observe that :

— The pessimistic expected utility $\text{UE}_*(d)$ is minimized when $p_i = p_{\text{sup}}$ (i.e., when the probability of cloudiness is at its maximum), because $1 - p_i$ is minimized.

— The optimistic expected utility $\text{UE}^*(d)$ is maximized when $p_i = p_{\text{inf}}$ (i.e., when the probability of cloudiness is at its minimum), because $1 - p_i$ is maximized.

4 Experimentation

In this section, we present the experiments conducted to test our proposed model under uncertainty. We implemented the model using the Zimpl modeling language and solved it using SCIP, an open-source optimization solver. Zimpl allowed us to concisely formulate the Binary Integer Programming (BIP) problem, while SCIP provided efficient computational methods to solve it. We tested the model across five different datasets of images, each with varying parameters such as image types, acquisition times, and probabilities of cloud coverage and instrument failure. This experimentation evaluates the effectiveness of our decision-making model in handling the uncertainties inherent in cloud coverage and instrument reliability.

FIGURE 9 – Scip Solver

4.1 Decision Variables

We define the following decision variables used in the optimization model :

— **selection**$_i \in \{0,1\}$: Binary variable indicating whether image i is selected for acquisition. **selection**$_i = 1$ if image i is selected, and 0 otherwise.

— **assignedTo**$_{i,j} \in \{0,1\}$: Binary variable indicating whether image i is assigned to instrument j. **assignedTo**$_{i,j} = 1$ if image i is assigned to instrument j, and 0 otherwise.

All decision variables are binary, reflecting the discrete nature of the scheduling problem where each image is either selected or not, and each assignment is either made or not.

4.2 Constraints

Memory Constraint :

$$\sum_{i \in \boldsymbol{s}_{\text{im}}} pm_i \cdot \text{selection}_i \leq PM_{\max}$$

```
subto memory:
    sum <i> in images: pm[i] * selection[i] <= PMmax;
```

Transition Constraint :

$$\forall i_1, i_2 \in \boldsymbol{s}_{\text{im}},\ j \in \boldsymbol{s}_{\text{ins}},\ i_1 < i_2 :$$

$$|dd_{i_1,j} - dd_{i_2,j}| \cdot VI < DU \cdot VI + |an_{i_1,j} - an_{i_2,j}|$$

$$\Downarrow$$

$$\text{assignedTo}_{i_1,j} + \text{assignedTo}_{i_2,j} \leq 1$$

```
subto transition:
    forall <i1, i2, j> in images * images * instruments
        with i1 < i2
        and abs(dd[i1, j] - dd[i2, j]) * VI < DU * VI + abs(an[i1, j] - an[
    i2, j]):
        assignedTo[i1, j] + assignedTo[i2, j] <= 1;
```

Mono Correspondence Constraint :

$$\forall\, i \in \boldsymbol{s}_{\text{im}}, \quad \text{if } ty_i = 1$$

$$\Downarrow$$

$$\sum_{j \in \boldsymbol{s}_{\text{ins}}} \text{assignedTo}_{i,j} = \text{selection}_i$$

```
subto correspondencemono:
    forall <i> in images with ty[i] == 1:
        sum <j> in instruments: assignedTo[i, j] == selection[i];
```

Stereo Correspondence Constraints :

$$\forall\, i \in \boldsymbol{s}_{\text{im}}, \quad \text{if } ty_i = 2$$

$$\Downarrow$$

$$\begin{cases} \text{assignedTo}_{i,1} = \text{selection}_i \\ \text{assignedTo}_{i,2} = 0 \\ \text{assignedTo}_{i,3} = \text{selection}_i \end{cases}$$

```
subto correspondencestereo:
    forall <i> in images with ty[i] == 2:
        assignedTo[i, 1] == selection[i];
        assignedTo[i, 2] == 0;
        assignedTo[i, 3] == selection[i];
```

4.3 Objective Function

In Section 3.4, we formulated the expected utility for acquiring a *mono* image i using instrument j, considering uncertainties due to cloudiness and instrument failure. The expected utility was defined as :

$$\text{UE}_p(d_i) = pa_i \times (1 - p_i) \times (1 - p_j)$$

where :

— pa_i is the profit (price) of image i.

— p_i is the probability that image i is cloudy, which lies within the interval $[p_{\text{inf},i}, p_{\text{sup},i}]$.

— p_j is the constant failure probability of instrument j.

To extend this to both *mono* and *stereo* images, we introduce the assignment variables $\text{assignedTo}_{i,j}$, which indicate whether image i is assigned to instrument j. We multiply by $\text{assignedTo}_{i,j}$ to account for only the assigned instruments. Thus, the expected utility for image i becomes :

$$\text{UE}_p i(d_i) = pa_i \times (1 - p_i) \times \sum_{j \in \boldsymbol{s}_{\text{ins}}} \left((1 - p_j) \times \text{assignedTo}_{i,j}\right)$$

Since we have two types of images—*mono* ($ty_i = 1$) and *stereo* ($ty_i = 2$)—we need to normalize the profit by dividing by ty_i to accurately represent the expected utility per image. The normalized expected utility is :

$$\mathrm{UE}_p(d_i) = \frac{1}{ty_i} \times pa_i \times (1 - p_i) \times \sum_{j \in \boldsymbol{s}_{\mathrm{ins}}} \left((1 - p_j) \times \mathrm{assignedTo}_{i,j}\right)$$

To compute the total expected utility, we sum over all images and include the $\mathrm{selection}_i$ variable to consider only the selected images :

$$\text{Maximize } \mathrm{UE}_p(d) = \sum_{i \in \boldsymbol{s}_{\mathrm{im}}} \left(\frac{1}{ty_i} \times \mathrm{selection}_i \times pa_i \times (1 - p_i) \times \sum_{j \in \boldsymbol{s}_{\mathrm{ins}}} \left((1 - p_j) \times \mathrm{assignedTo}_{i,j}\right) \right)$$

However, this objective function still depends on p_i, which lies within the interval $[p_{\mathrm{inf},i}, p_{\mathrm{sup},i}]$. Referring back to Section 3.4, we have shown that :

- Under the **pessimistic** criterion, the worst-case expected utility occurs when $p_i = p_{\mathrm{sup},i}$.
- Under the **optimistic** criterion, the best-case expected utility occurs when $p_i = p_{\mathrm{inf},i}$.

Therefore, we define two different objective functions :

Pessimistic Objective Function :

$$\text{Maximize } \mathrm{UE}_*(d) = \sum_{i \in \boldsymbol{s}_{\mathrm{im}}} \left(\frac{1}{ty_i} \times \mathrm{selection}_i \times pa_i \times (1 - p_{\mathrm{sup},i}) \times \sum_{j \in \boldsymbol{s}_{\mathrm{ins}}} \left((1 - p_j) \times \mathrm{assignedTo}_{i,j}\right) \right)$$

Optimistic Objective Function :

$$\text{Maximize } \mathrm{UE}^*(d) = \sum_{i \in \boldsymbol{s}_{\mathrm{im}}} \left(\frac{1}{ty_i} \times \mathrm{selection}_i \times pa_i \times (1 - p_{\mathrm{inf},i}) \times \sum_{j \in \boldsymbol{s}_{\mathrm{ins}}} \left((1 - p_j) \times \mathrm{assignedTo}_{i,j}\right) \right)$$

Implementation in Zimpl :

The objective function can be implemented in Zimpl as :

```
maximize valeur:
    sum <i> in images :
        (1 / ty[i]) * selection[i] * pa[i] * (1 - P[i]) *
        (
            sum <j> in instruments:
                assignedTo[i,j] * (1 - Pfail[j])
        );
```

In the Zimpl code :

- $P[i]$ represents $p_{\mathrm{sup},i}$ for the pessimistic case or $p_{\mathrm{inf},i}$ for the optimistic case.

The next section will discuss how the two approaches affects the solution

4.4 Results

We applied our optimization model to five datasets (SPOT1 to SPOT5), obtaining solutions under both pessimistic and optimistic scenarios. The objective function values for each dataset are presented in Table 11.

Dataset	Pessimistic Obj	Optimistic Obj
SPOT1	44.00	60.00
SPOT2	60.00	60.00
SPOT3	60.00	60.00
SPOT4	279.00	310.00
SPOT5	340.69	419.61

TABLE 11 – Objective Function Values under Pessimistic and Optimistic Scenarios

Discussion The results in Table 11 show the optimal expected utilities obtained under both pessimistic and optimistic scenarios for each dataset. For SPOT1, the optimistic scenario yields

an objective value of 60.00, which matches the result obtained without considering uncertainties (as found in Section 2.2). This occurs because the lower bound of the cloudiness probability $p_{\text{inf}} = 0$, eliminating the impact of cloudiness in the optimistic case. Therefore, the expected utility is maximized, and uncertainties do not affect the outcome under the optimistic scenario. The pessimistic value is lower due to the upper bound $p_{\text{sup}} > 0$, reflecting the potential risk of cloudiness. For SPOT2 and SPOT3, both scenarios yield the same objective value (60.00), because there are no uncertainties affecting these datasets, actually $p_{\text{inf}} = p_{\text{sup}} = 0$ for all images in SPOT2 and SPOT3, so the expected utility remains. For SPOT4 and SPOT5, we observe that the pessimistic expected utility is less than the optimistic expected utility, which is intuitively true because higher cloudiness probabilities in the pessimistic scenario reduce the expected profits. The differences between the pessimistic and optimistic values highlight the significant impact of uncertainty on the expected utilities. Decision-makers must consider these variations when planning image acquisitions to balance potential profits against risks.

5 Conclusion

In this paper, we addressed the acquisition planning problem for a single Earth Observation Satellite under uncertainty. We modeled uncertainties in cloud coverage and instrument failures using decision theory with imprecise probabilities, employing pessimistic and optimistic criteria to guide decision-making. Our approach successfully optimizes the scheduling of image acquisitions, balancing potential profits against risks. While this study focuses on a single satellite, the proposed framework can be extended to scenarios involving multiple satellites, where satellites can transmit acquired data while maintaining their trajectories. Additionally, future work may explore long-term management strategies, enhancing the model's applicability to more complex and realistic satellite operations.

Références

1. N. Bianchessi, J.-F. Cordeau, J. Desrosiers, G. Laporte, and V. Raymond, "A heuristic for the multi-satellite, multi-orbit and multi-user management of earth observation satellites," *European Journal of Operational Research*, vol. 177, no. 2, pp. 750–762, 2007.
2. J.-F. Cordeau and G. Laporte, "Maximizing the value of an earth observation satellite orbit," *Journal of the Operational Research Society*, vol. 56, no. 8, pp. 962–968, 2005.
3. E. Bensana, M. Lemaitre, and G. Verfaillie, "Earth observation satellite management," *Constraints*, vol. 4, no. 3, pp. 293–299, 1999.
4. M. A. Mansour and M. M. Dessouky, "A genetic algorithm approach for solving the daily photograph selection problem of the spot5 satellite," *Computers Industrial Engineering*, vol. 58, no. 3, pp. 509–520, 2010. Supply, Production and Distribution Systems.
5. A. Bouillon, E. Breton, F. De Lussy, and R. Gachet, "Spot5 geometric image quality," in *IGARSS 2003. 2003 IEEE International Geoscience and Remote Sensing Symposium. Proceedings (IEEE Cat. No.03CH37477)*, vol. 1, pp. 303–305 vol.1, 2003.
6. C. He, Y. Dong, H. Li, and Y. Liew, "Reasoning-based scheduling method for agile earth observation satellite with multi-subsystem coupling," *Remote Sensing*, vol. 15, no. 6, 2023.
7. X. Wang, R. Leus, and C. Han, "Fixed interval scheduling of multiple earth observation satellites with multiple observations," in *2018 9th International Conference on Mechanical and Aerospace Engineering (ICMAE)*, pp. 28–33, 2018.
8. W. Zhu, X. Hu, W. Xia, and H. Sun, "A three-phase solution method for the scheduling problem of using earth observation satellites to observe polygon requests," *Computers Industrial Engineering*, vol. 130, pp. 97–107, 2019.
9. G. Peng, R. Dewil, C. Verbeeck, A. Gunawan, L. Xing, and P. Vansteenwegen, "Agile earth observation satellite scheduling : An orienteering problem with time-dependent profits and travel times," *Computers Operations Research*, vol. 111, pp. 84–98, 2019.
10. J. Wang, E. Demeulemeester, and D. Qiu, "A pure proactive scheduling algorithm for multiple earth observation satellites under uncertainties of clouds," *Computers Operations Research*, vol. 74, pp. 1–13, 2016.
11. X. Wang, Y. Gu, G. Wu, and J. R. Woodward, "Robust scheduling for multiple agile earth observation satellites under cloud coverage uncertainty," *Computers Industrial Engineering*, vol. 156, p. 107292, 2021.
12. B. Du and S. Li, "A new multi-satellite autonomous mission allocation and planning method," *Acta Astronautica*, vol. 163, pp. 287–298, 2019. Fourth IAA Conference on Dynamics and Control of Space Systems (DYCOSS2018).

13. L. J. Savage, *The Foundations of Statistics.* John Wiley & Sons, 1954.
14. A. Wald, *Statistical Decision Functions.* John Wiley & Sons, 1950.
15. D. Ellsberg, "Risk, ambiguity, and the savage axioms," *The Quarterly Journal of Economics*, vol. 75, no. 4, pp. 643–669, 1961.
16. L. A. Zadeh, "Fuzzy sets as a basis for a theory of possibility," *Fuzzy Sets and Systems*, vol. 1, no. 1, pp. 3–28, 1978.
17. G. A. Papadopoulos, *Stochastic Programming and the Theory of Decision Making under Uncertainty*, vol. 79 of *Lecture Notes in Economics and Mathematical Systems.* Springer, 1973.